



2nd Advanced Optical Metrology Compendium

Advanced Optical Metrology

Geoscience | Corrosion | Particles | Additive Manufacturing: Metallurgy, Cut Analysis & Porosity



EVIDENT
OLYMPUS

WILEY

The latest eBook from
Advanced Optical Metrology.
Download for free.

This compendium includes a collection of optical metrology papers, a repository of teaching materials, and instructions on how to publish scientific achievements.

With the aim of improving communication between fundamental research and industrial applications in the field of optical metrology we have collected and organized existing information and made it more accessible and useful for researchers and practitioners.

EVIDENT
OLYMPUS

WILEY

Clathrate-Like Alkali and Alkaline-Earth Metal Borides: A New Family of Superconductors with Superior Hardness

Shuai Han, Linchao Yu, Yunxian Liu,* Bo Zhao, Chao Wang, Xin Chen, Yongsheng Zhang,* Runze Yu, and Xiaobing Liu*

Conventional hard and superhard materials, such as diamond and cubic boron nitride, are attractive for fundamental material science and practical industrial application, but severely limited by their poor electrical conductivity. Therefore, it is desirable to design and fabricate novel materials for superior hardness and conductivity. Herein, a class of hard superconductors in alkali or alkaline-earth metal (AM) borides, namely AMB_7 , constituted by a B_{23} cage with one centered metal atom (Li, Na, K, Mg, Ca, and Sr) is reported, which is the first stable clathrate structure in AMB systems. The theoretical calculations demonstrate that all these pressure-stabilized clathrate structures can be quenched down to ambient conditions, which provides an essential prerequisite for experimental synthesis at moderate pressures. Among them, the highest hardness and maximum superconducting transition temperature (T_c) value are achieved in SrB_7 (25.1 GPa) and MgB_7 (29.3 K), respectively. Interestingly, the results show that KB_7 simultaneously behaves high hardness (22.5 GPa) and superconducting transition temperature ($T_c \approx 26.2$ K). This study opens up a new way to search and design novel superconductors with favorable mechanical properties under high pressure and high-temperature conditions.

1. Introduction

Search for hard and superhard materials with superior conductivity is always of great importance in fundamental material science and practical industrial application. The 3D covalent rigid

bonding networks of carbon atoms make diamond attractive as the hardest solid in nature. Such strong and short covalent bonds tend to localize the free electrons in diamond, thus leading to a wide band gap (5.47 eV), which behaves as an insulator.^[1] Transition-metal borides (TMB) have attracted wide scientific interest in searching for hard and superhard conducting solids (e.g., ReB_2 , WB_4) in recent decades.^[2–5] The existing strong B–B covalent bonding network can strengthen the mechanical properties, whilst the TM–TM bonds are usually beneficial to the electron transportation. These behaviors lead to the discovery of a series of hard and superhard TMB materials with semiconducting,^[6] metallic^[7,8], and even superconducting^[9–12] properties. Such unique properties enable potential development for electronic device applications for certain extreme conditions, such as high pressure and dynamic environments. However, previous experiments revealed that fabrication of such TMB compounds usually requires extremely high pressure and temperature conditions, e.g., FeB_4 (8–18 GPa), LaB_8 (108 GPa and 2100 K), MnB_4 (10–12 GPa and 1873 K), and $\text{Mo}_{0.75}\text{B}_3$ (15 GPa and 2023 K),^[10,11,13,14] resulting in limited sample size by several millimeters, which has severely hampered their industrial fabrication and practical application as devices.

Alkali or alkaline-earth metals (AM) possessing high chemical activity are expected to form stable AM borides (AMB) with uncommon stoichiometries and exotic properties at the relatively lower P–T condition, which can be due to the effective adjusting of *d*-electron bands at pressures.^[15–18] For instance, metallic calcium borides of *P4/mmb* CaB_4 ^[19] and *Pm-3m* CaB_6 ^[20] have been fabricated at 1–2 GPa and about 1300 K, which is much lower than that required P–T conditions for the synthesis of TMB systems. Very recently, we also successfully produced a novel honeycomb-like NaB_4 structure at 1.5 GPa and 1000 K,^[21] predicted by our theoretical calculations as a pressure-stabilized phase at 80 GPa that can be quenchable under ambient conditions,^[22] enabling fabrication of large-size productions (several centimeters in diameter). The NaB_4 sample exhibits strong B–B covalent bonds with hardness up to 26 GPa, which can be comparable to previously reported TMB materials.^[13,23,24] Most interestingly, the produced NaB_4 sample exhibits a superconductor with superconducting transition temperature (T_c) of 4 K

S. Han, L. Yu, Y. Liu, C. Wang, X. Chen, Y. Zhang, X. Liu
Laboratory of High Pressure Physics and Material Science

School of Physics and Physical Engineering
Qufu Normal University
Qufu, Shandong Province 273165, China

E-mail: yunxianliu@qfnu.edu.cn; yshzhang@qfnu.edu.cn;
xiaobing.phy@qfnu.edu.cn

S. Han, R. Yu
Center for High Pressure Science and Technology Advanced Research
Beijing 100094, China

Y. Liu, C. Wang, X. Chen, Y. Zhang, X. Liu
Advanced Research Institute of Multidisciplinary Sciences
Qufu Normal University
Qufu, Shandong Province 273165, China

B. Zhao
State Key Laboratory of Superhard Materials
Jilin University
Changchun, Jilin Province 130012, China

The ORCID identification number(s) for the author(s) of this article
can be found under <https://doi.org/10.1002/adfm.202213377>.

DOI: 10.1002/adfm.202213377

by removing part of sodium atoms, and undergoes an unusual superconducting-metallic-semiconducting transition by applying external stress up to 100 GPa.

On the basis of previous results,^[6,25,26] the formation of covalent bonds between the metal and boron atoms is a disadvantage of the superconducting behaviors, while the AM atoms usually tend to form ionic bonds with boron atoms at high pressures.^[21,22,27,28] MgB₂ structure containing dominated B–B bonds in the company of ionic Mg–B bonds, exhibits strong coupling between electrons at the Fermi level and phonons from the covalent boron network,^[27] thus resulting in a record T_c value of 39 K in all reported borides. Similar phenomenon is also observed in NaB₆ ($T_c = 15.7$ K) and KB₆ ($T_c = 14.6$ K) superconductors.^[28] Thus we expect to search for new superconducting phases with superior mechanical properties in AMB phases at high pressures, which simultaneously contain ionic AM–B bonds and strong covalent B–B bonding framework.

It has been found that the clathrate-like boron framework in reported TMB systems usually shows excellent mechanical properties (hardness and strength),^[9,13,29,30] together with metallic properties (WB₁₂, TiB₁₂),^[29] even behaving as superconductors (YB₁₂, ZrB₁₂, LaB₈) with $T_c \approx 4\text{--}14$ K.^[9,13,30] However, thus far there is still a lack of similar clathrate-like structures for AMB systems in previous theoretical and experimental works. Elemental calcium (Ca) is one potential candidate because of its suitable atomic radius (1.80 Å) and high reactive activity with boron (i.e., CaB, CaB₂, CaB₄, and CaB₆).^[19,20,31] Considering the requirement for large boron content in clathrate-like framework,^[9,13,29,30] we thus focus our investigation in this work on the clathrate structures in the CaB_x ($x = 1\text{--}12$) systems throughout the pressure range of 0–200 Gpa by the USPEX and CAIYPSO codes.^[32–37] Here we report a pressure-stabilized *Cmcm* CaB₇ phase at 141 Gpa, constituted by a B₂₃ cage with one centered calcium atom, behaving as the first clathrate structure in AMB systems. This structure can be quenched down to ambient conditions with a hardness of 20.4 Gpa and T_c value of 7.7 K. Moreover, our calculation reveals that such structure remains stable after substituting the calcium atom with other AM atoms, including lithium (Li), sodium (Na), kalium (K), magnesium (Mg), and strontium (Sr), forming a new hard AMB₇ superconducting family. The clathrate-like KB₇ is predicted to simultaneously behave high hardness (22.5 GPa) and superconducting transition temperature ($T_c \approx 26.2$ K). The highest hardness and maximum T_c values have been achieved up to 25.1 GPa of SrB₇ and 29.3 K of MgB₇, respectively. This study paves a new routine for the design of hard superconductors in borides, thus stimulating further experimental synthesis in the future.

2. Results and Discussion

We performed extensive structure search for B-rich Ca–B systems with variable compositions by applying external pressures in the range of 0–200 GPa, as shown in the convex hull and phase diagrams of **Figure 1a** and Figures S1–S3 (Supporting Information). The thermodynamic stabilities of all studied phases were analyzed with respect to the elemental calcium and boron. Besides the previously known CaB, CaB₂, CaB₄,

and CaB₆,^[31] two novel stable stoichiometries, namely CaB₅ and CaB₇, also can be stabilized at pressures of 126 and 156 GPa (Figure S3, Supporting Information), respectively. More structural details of CaB, CaB₂, CaB₄, CaB₅, and CaB₆ phases can be seen in Figure S4 (Supporting Information). It is interesting to find that our predicted CaB₇ phase is composed of 3D boron clathrate structures, as we expected. This is the first time to find a stable clathrate-like structure in the AMB systems. Therefore, we will focus our analysis and discussion on the CaB₇ structure in the following parts.

Figure 1b,c shows that the CaB₇ adopts an orthorhombic structure with the space group of *Cmcm*, where boron atoms form contiguous face-sharing B₂₃ cages, while calcium atoms are located in the center position. This is the first time to observe B₂₃ cages in metal borides, while B₂₄ and B₂₆ cages were previously reported in MB₁₂ (e.g., *Fm-3m* UB₁₂, *I4/mmm* ScB₁₂) and *R-3m* LaB₈,^[13,38] respectively. The detailed structural information is summarized in Table S1 (Supporting Information). There are three inequilibrium B sites in this cage, namely B1, B2, and B3 (Figure S5, Supporting Information). The B₂₃ cages are constructed from two planar hexagons, four pentagons, four quadrilaterals, and fourteen triangles, that possess B–B bonds with a length of 1.60–1.76 Å at 150 GPa. We determined the dynamical stability of clathrate CaB₇ using the phonon calculations in the pressure range of 0–200 GPa (Figure S6, Supporting Information). No imaginary frequency in all phonon dispersions can be seen throughout all studied pressure range. The ab initio MD simulations (Figure S7, Supporting Information) show these clathrate structures still keep stable at 0 GPa and 300 K. These results manifest that the predicted *Cmcm* CaB₇ structure can be quenchable after releasing the pressure down to ambient conditions, which provides high possibility for the experimental synthesis at relatively moderate P–T conditions (e.g., NaB₄, DyH₃, and uranium polyhydrides).^[21,22,39,40] The length of B–B bonds expand to 1.80–2.09 Å at 0 GPa from 1.60–1.76 Å at 150 GPa, which is comparable to that of the well-known α -B (1.67–2.00 Å)^[41] and β -B (1.66–1.90 Å) phases,^[42] suggesting the formation of strong covalent network in the B₂₃ cage, an essential element of superior mechanical properties.

The electron localization function (ELF) in **Figure 1d** and **Figure S9** (Supporting Information) reveals that the localized function among boron atoms in the B₂₃ cage is within 0.72–0.93, which is above 0.5 for covalent B–B interaction in general, and the larger value indicates stronger covalent binding.^[43] The calculated crystal orbital Hamiltonian population (COHP) in **Figure S10** (Supporting Information) shows fully occupied bonding states below the Fermi level, evidencing the formation of strong covalent B–B bonds in the B₂₃ cages. The integrated COHP values between B–B and Ca–B pairs are –4.63 and –0.47 eV per pair, respectively. More importantly, we notice that pure ionic Ca–B bonds are formed in the CaB₇ structure, in absence of charge localization, which is expected to be beneficial for electron transport between the B cages and the centered Ca atoms. Each clathrate B₂₃ cage can accept 1.79 electrons from the 13 neighboring Ca atoms, analyzed by Bader charge analysis (Table S2, Supporting Information).

To examine the electron transport properties of *Cmcm* CaB₇, we calculated its electronic band structures and the projected density of states (PDOS). **Figure 2a** illustrates the metallic

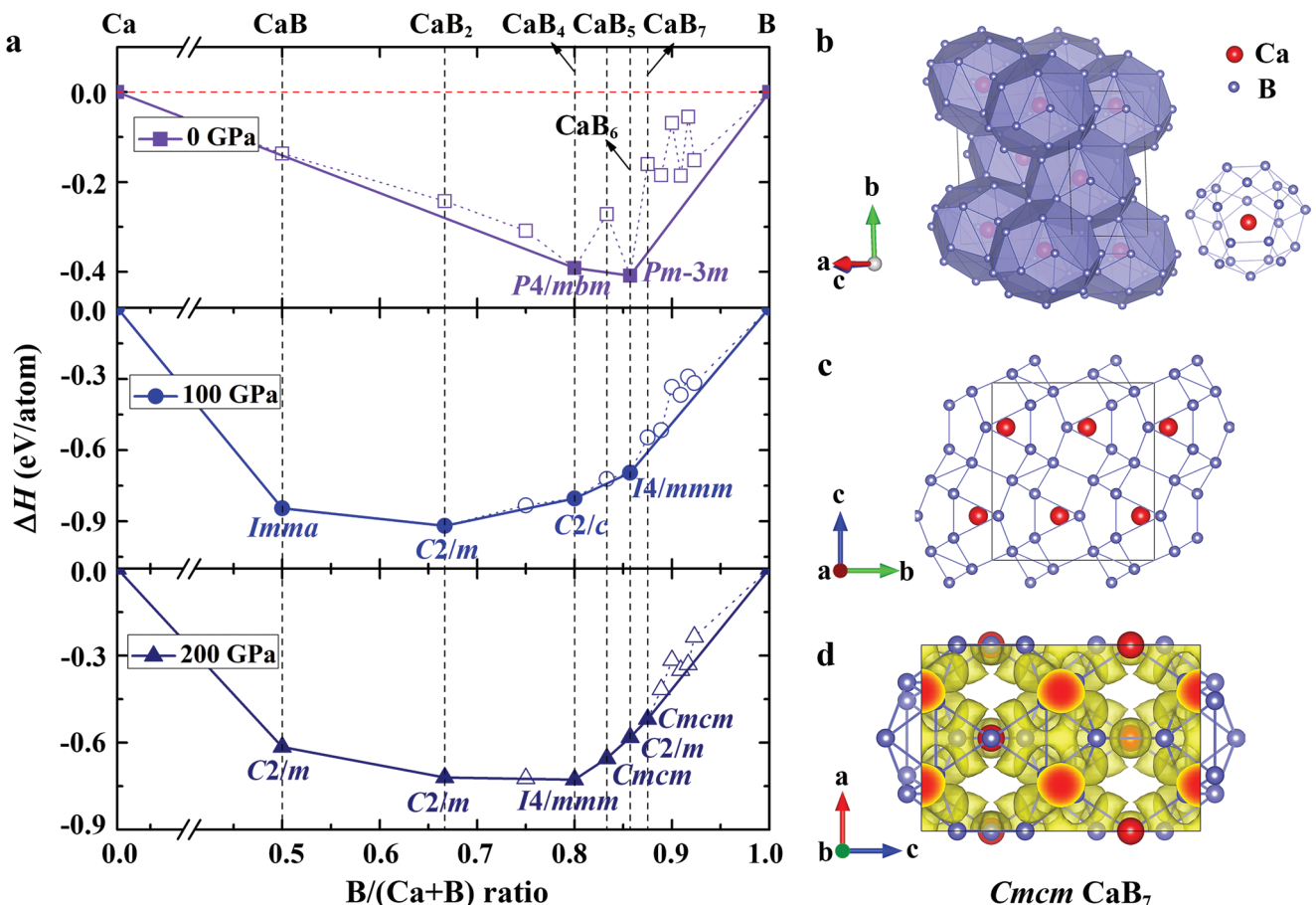


Figure 1. Convex hull of B-rich calcium borides and the structure motif of *Cmcm* CaB₇. a) Formation enthalpies of predicted CaB_x ($x = 1\text{--}12$), with respect to Ca and B at 0, 100, and 200 GPa. The solid and open symbols in the phase diagrams represent the thermodynamically stable and unstable compounds, respectively. b) and c) are the crystal structure of clathrate *Cmcm* CaB₇ from different view directions. The red and violet balls denote Ca and B atoms, respectively. d) The 3D ELF with isosurface value of 0.7 at 150 GPa.

nature of CaB₇ structure with four bands (from B cages and Ca atoms) crossing the Fermi level. The flat bands are formed along the Y→R direction, while steep bands can be seen along the Y→S and S→X directions. The DOS at Fermi level in Figure 2b is mainly originated from B1-*p*, B2-*p*, B3-*p*, and Ca-*d* orbitals, while little contributions from Ca-*p* and B-*s* orbitals. No component of Ca-*s* state can be seen at the Fermi level, indicating the transferred electrons for B₂₃ cages are from the 4s orbit of Ca atoms. Figure 2c shows a clear Fermi surface nesting appears in the CaB₇ Brillouin zone along the Z→T and Γ →Y directions. Such features can lead to high electronic DOS near the Fermi level, raising possibility of the formation of Cooper pairs and strengthening the electron–phonon coupling (EPC), which thus were expected to result in superconductors.^[21,44–46]

We further calculated the superconducting transition temperature (T_c) of CaB₇ structure by the Allen–Dynes modified McMillan equation.^[47] For reasonable comparison with previously reported systems, we employed a commonly accepted value of Coulomb pseudopotential parameters ($\mu^* = 0.1$).^[13,48–50] The calculated pressure-dependent EPC constant (λ), the logarithmic average phonon frequency (ω_{\log}), and the electronic DOS at the Fermi level ($N(\varepsilon_f)$) at 0, 50, 100, 150, and 200 GPa are tabulated in Table S3 (Supporting Information). The values

of both λ and $N(\varepsilon_f)$ increase during the release of external pressures from 150 GPa, implying enhanced electron–phonon coupling and metallicity. The CaB₇ structure exhibits a superconductor with T_c of 77 K after quenching down to ambient pressure (Figure 2d).

To evaluate the mechanical properties, we then calculated the elastic constants (C_{ij}), bulk modulus (B), shear modulus (G), Pugh criterion (B/G), and Poisson's ratio (ν) of *Cmcm* CaB₇ structure. The obtained results are listed in Table S4 (Supporting Information). The calculated elastic constants meet the Born–Huang criteria,^[51] evidencing well mechanically stability of CaB₇ structure under ambient conditions. Using the empirical model $H_v = 2.0 (k^2 G)^{0.585} - 3.0$ ($k = G/B$, G is shear modulus, B is bulk modulus),^[52] the calculated Vicker hardness (H_v) of CaB₇ is 20.4 GPa. Then, we investigated the tensile and shear resistance to gain deeper insight into its mechanical properties. Figure 3a gives the tensile stress–strain relations along six directions, including [001], [010], [100], [101], [110], and [111] directions. The ideal tensile strength of CaB₇ corresponds to the [110] direction with the lowest peak value of 14.5 GPa, suggesting that the (100) plane is the preferred cleavage plane. Further investigations of ideal shear strength in the (100) plane along the [010], [001], and [011] shear slip directions are shown in Figure 3b. The weakest

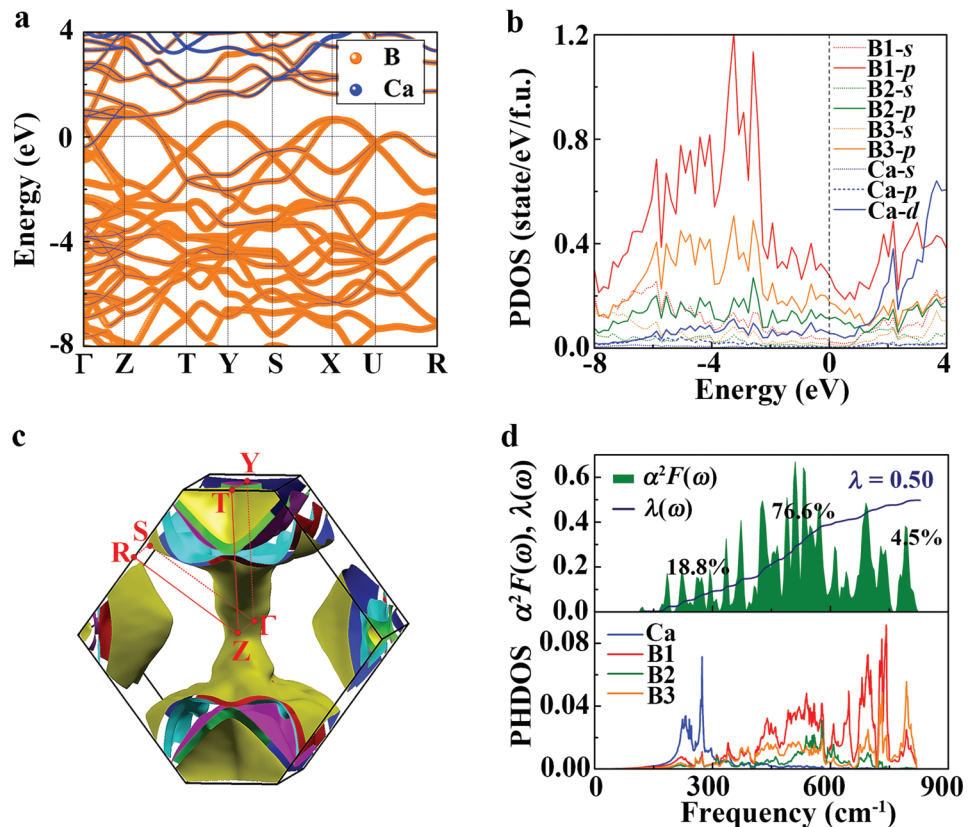


Figure 2. Electronic and superconducting properties of *Cmcm* CaB₇ at 0 GPa. a) Electronic band structures of *Cmcm* CaB₇. The horizontal dashed line indicates the Fermi level ϵ_F . b) Projected density of states (PDOS) of *Cmcm* CaB₇. The vertical dashed line indicates the Fermi level. c) The Fermi surface for *Cmcm* CaB₇. d) Eliashberg spectral function $\alpha^2F(\omega)$ (green area), frequency-dependent electron–phonon coupling parameters $\lambda(\omega)$ (blue line) and the projected phonon density of states (PHDOS) of *Cmcm* CaB₇.

shear strength of 12.3 GPa is obtained in the (100)[011] slip at a strain of 0.11. Figure 3c–d illustrates the evolutionary process of CaB₇ structure under shear strains of 0 (T_0), 0.11 (T_1), and 0.16 (T_2), respectively. We can see an increase of B2–B3 length from 2.04 Å (T_0) to 2.39 Å (T_1) at the strain (γ) of 0.11, then the B1–B1 and B1–B2 bonding lengths elongate from 1.90 Å (T_0) to 2.32 Å (T_2) and 1.85 Å (T_0) to 2.74 Å (T_2), respectively, with the increasing strain up to 0.16. From the calculated ELF, the electron localization within some B–B bonds gradually disappeared with increasing strain. As a result, the breaking of these major load-bearing bonds leads to a significant reduction in shear stress, that was shown in Figure 3b.

Motivated by above results, we further evaluated the stabilities of clathrate-like structure AMB₇ by replacing Ca atoms with other alkali metals (Li, Na, K, Rb, and Cs) and alkaline-earth metals (Be, Mg, Sr, and Ba). From our calculated enthalpies (ΔH) and phonon dispersion relations in Figures S11–S14 (Supporting Information), we found that similar clathrate structure can also be stabilized at pressures and quenched down to ambient conditions as LiB₇ (0–25 GPa), NaB₇ (0–50 GPa), KB₇ (0–100 GPa), MgB₇ (0–200 GPa), and SrB₇ (0–200 GPa). Suitable atomic radius and Pauling electronegativity are required for accommodation of metal atoms in the B clathrate.^[13] The Rb and Cs metal could not form stable clathrate-structural borides throughout pressures of 0–200 GPa, attributing to their large

atomic radius (Rb, 2.35 Å; Cs, 2.60 Å). The excessive Pauling electronegativity of Be atom (1.57) limits the charge transfer to B atom, therefore inhibiting the formation of B₂₃ cage, while Ba atom synchronously is affected by both two factors (atomic radius of 2.15 Å, Pauling electronegativity of 0.89).

Interestingly, our further calculated results in Table S5 (Supporting Information) demonstrate that all the predicted stable AMB₇ (AM = Li, Na, K, Mg, Ca, and Sr) structures exhibit as superconductors. Since the calculated T_c values of AMB₇ structures decrease with the increasing pressure, we compared the predicted T_c values for AMB₇ (AM = Li, Na, K, Mg, Ca, and Sr) systems at 0 GPa, as depicted in Figure 4, that CaB₇ < SrB₇ < N aB₇ < LiB₇ < KB₇ < MgB₇. The tendency of the total electronic DOS at the Fermi level $N(\epsilon_F)$ and λ is in agreement with that of the T_c , while the logarithmic average phonon frequency ω_{\log} goes opposite. This suggests that the superconducting behaviors are mainly determined by their $N(\epsilon_F)$ and λ values in AMB₇ structures. The high $N(\epsilon_F)$ and λ lead to a maximum T_c value of 29.3 K in MgB₇. Figure S15 (Supporting Information) shows the DOS at Fermi level can be dominantly attributed to B atoms in all AMB₇ structures. The contribution of PHDOS in Figure 2d and Figure S16 (Supporting Information) to the total λ can be divided into three regions: low-, middle-, and high-frequency in AMB₇. The high-frequency modes, corresponding to vibrations of B1 and B2 atoms, contribute <5%, while the dominated

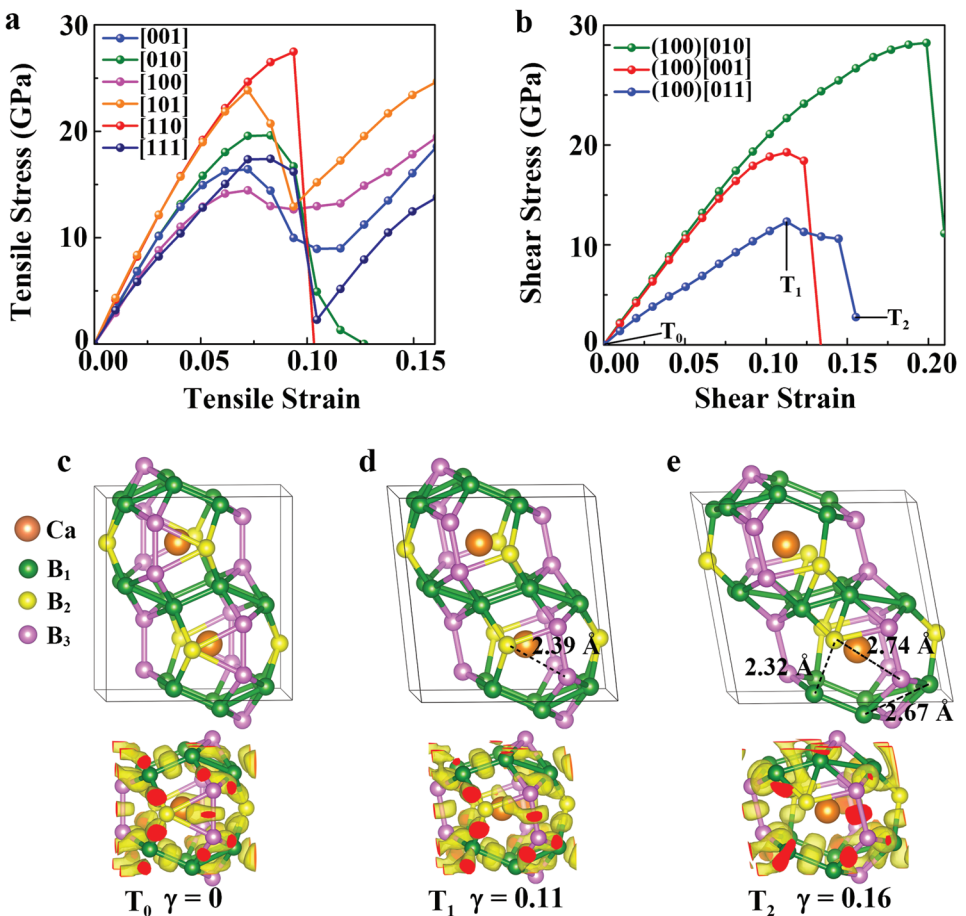


Figure 3. a) Calculated tensile stress–strain relationships of CaB₇. b) Calculated shear stress–strain relationships in the (100) easiest cleavage plane of CaB₇. c–e) Key structural snapshots and electron localization functions of CaB₇ under the (100) <011> shear strains with an isovalue of 0.75.

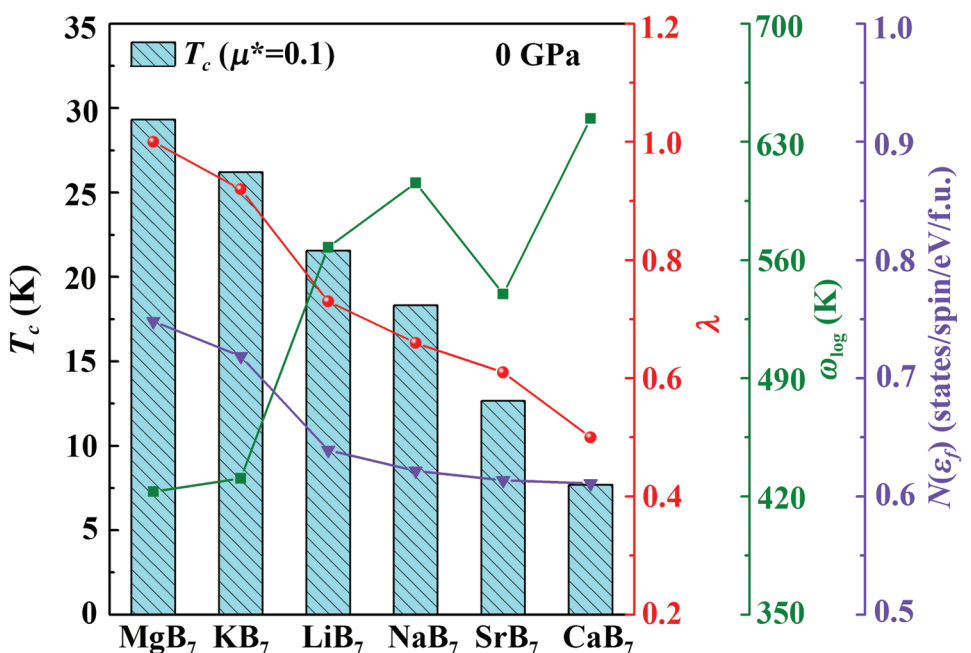


Figure 4. Calculated superconducting parameters for MgB₇, KB₇, LiB₇, NaB₇, SrB₇, and CaB₇ at 0 GPa. The superconducting critical temperature T_c (the black shadowed bars), EPC parameter (λ , the red line), the logarithmic average phonon frequency ω_{\log} (the green line), and the total electronic DOS at the Fermi level $N(\epsilon_F)$ (the purple line).

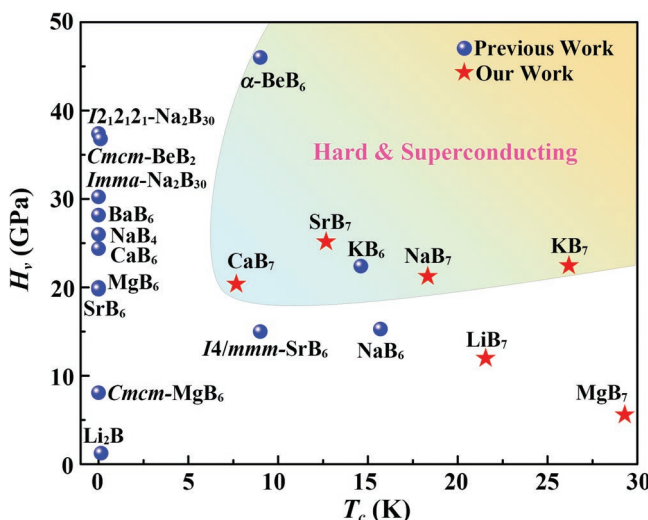


Figure 5. The Vickers hardness (H_v) and superconducting transition temperatures (T_c) of different alkali metal, alkaline earth metal borides at ambient pressure.

contributions are derived from the low- (AM and B atoms) and middle-frequency (B atoms) regions by 20–40% and 50–70%, respectively. Therefore, the superconducting behaviors in our predicted AMB₇ structures are mainly originated from the electron-phonon coupling of boron networks. Most importantly, we can see clearly an increase of the total λ with the increasing proportion of low-frequency modes, which strongly demonstrates the interaction between AM atoms and B₂₃ clathrate cage plays a key role in determining the T_c values of the structures.

The Vickers hardness values of AMB₇ structures are calculated as MgB₇ < LiB₇ < CaB₇ < NaB₇ < KB₇ < SrB₇. The SrB₇ shows the highest hardness as 25.1 GPa, which is attributed to the enhanced bond directionality and orbital strength by the contribution of d electrons in Sr atoms.^[53,54] Figure 5 summarizes the calculated H_v and T_c values of our predicted AMB₇ (AM = Li, Na, K, Mg, Ca, and Sr) structures, in comparison with that of previously reported works.^[28,55–61] Four new phases of CaB₇, SrB₇, NaB₇, and KB₇ can be seen as hard superconductors with hardness above 20 Gpa. Moreover, it can be clearly noted that the clathrate KB₇ can be expected to be a suitable candidate that simultaneously behaving a high hardness of 22.5 Gpa and T_c value of 26.2 K. Our results demonstrate that the clathrate-like boron framework in combination with ionic AM–B bonds plays key role in creating hard superconducting phases in AMB systems.

3. Conclusion

We have successfully found a new family of AMB₇ structures, which are constituted by a B₂₃ cage with one centered metal atom (Li, Na, K, Mg, Ca, and Sr) by first principle calculations. This is the first time to report a stable clathrate structure in AMB systems. These clathrate structures can be stabilized under high pressure conditions, and keep stable after quenching down to ambient conditions, which enables the future experimental synthesis of large-size productions at mod-

erate pressures, an essential prerequisite for device application. The highest hardness and maximum T_c value are achieved in SrB₇ (25.1 Gpa) and MgB₇ (29.3 K), respectively, while the KB₇ simultaneously behaves as one superior hard superconductor ($H_v = 22.5$ Gpa, $T_c = 26.2$ K). This study could open up a new way to search and design novel superconductors with favorable mechanical properties in AMB systems under high pressure and high-temperature conditions.

4. Computational Method

For comprehensive forecast, structure searches of Ca–B system were performed using Universal Structure Predictor: Evolutionary Xtallography (USPEX) code and Crystal structure AnaLYsis Particle Swarm Optimization (CALYPSO) code.^[32–37] Such methods had been successfully employed in various systems.^[13,48–50,62] Global structural optimization and electronic properties were carried out within the framework of density functional theory (DFT) as implemented in the Vienna ab initio simulation package (VASP) code.^[63] The Perdew–Burke–Ernzerhof generalized gradient approximation (GGA–PBE)^[64] was chosen for the exchange–correlation functional. We used all-electron projector–augmented wave (PAW)^[65] pseudopotentials with $3s^23p^64s^2$ and $2s^22p^1$ electrons as valence for Ca and B atoms, respectively. The cutoff energy of 500 eV and a Monkhorst–Pack scheme^[66] with a dense k-point grid spacing of $2\pi \times 0.03 \text{ \AA}^{-1}$ were chosen in order to yield an excellent convergence for the Gibbs free energy. The crystal orbital Hamiltonian population COHP was also calculated using LOBSTER,^[67] which is a bond-detecting tool used to differentiate covalent and non-covalent bonding in chemistry. The electron localization function (ELF)^[42] was used to describe and visualize chemical bonds in molecules and solids. And Bader charge analysis^[68] was performed to determine charge transfer between B cages and Ca atoms. Phonon calculations by using the finite displacement approach^[69] were performed, as implemented in the PHONOPY code.^[70] Electron–phonon coupling calculations for superconductivity were employed using the QUANTUM–ESPRESSO package.^[71] Ab initio molecular dynamics (MD) simulations were performed using the Nose–Hoover thermostat lasted for 9 ps with a time step of 1.5 fs.^[72] We estimated the bulk modulus B (GPa) and shear modulus G (GPa), from the calculated elastic constants by using the Voigt–Reuss–Hill approximation.^[73]

Supporting Information

Supporting Information is available from the Wiley Online Library or from the author.

Acknowledgements

This work was supported by the National Natural Science Foundation of China (no. 52102335, 52172212, and 11974208), Shandong Provincial Natural Science Foundation (no. ZR2021MA050, ZR2021YQ03, ZR2020YQ05, and 2019KJJ020) and by Open Project of State Key Laboratory of Superhard Materials, Jilin University (no. 202108). Theoretical calculations were performed in the High Performance Computing Center (HPCC) of Qufu Normal University.

Conflict of Interest

The authors declare no conflict of interest.

Data Availability Statement

The data that support the findings of this study are available in the supplementary material of this article.

Keywords

clathrate-like borides, first principle calculations, hard superconductors, high pressure

Received: November 16, 2022

Revised: December 17, 2022

Published online:

- [1] X. Liu, X. Chen, D. J. Singh, R. A. Stern, J. Wu, S. Petitgirard, C. R. Bina, S. D. Jacobsen, *Proc. Natl. Acad. Sci. USA* **2019**, *116*, 7703.
- [2] H. Y. Chung, M. B. Weinberger, J. B. Levine, A. Kavner, J. M. Yang, S. H. Tolbert, R. B. Kaner, *Science* **2007**, *316*, 436.
- [3] N. Dubrovinskaia, L. Dubrovinsky, V. L. Solozhenko, *Science* **2007**, *318*, 1550.
- [4] H. Y. Chung, M. B. Weinberger, J. B. Levine, R. W. Cumberland, A. Kavner, J. M. Yang, S. H. Tolbert, R. B. Kaner, *Science* **2007**, *318*, 1550.
- [5] R. Mohammadi, A. T. Lech, M. Xie, B. E. Weaver, M. T. Yeung, S. H. Tolbert, R. B. Kaner, *Proc. Natl. Acad. Sci. USA* **2011**, *108*, 10958.
- [6] Q. Wang, Q. Zhang, M. Hu, M. Ma, B. Xu, J. He, *Phys. Chem. Chem. Phys.* **2014**, *16*, 22008.
- [7] R. W. Cumberland, M. B. Weinberger, J. J. Gilman, S. M. Clark, S. H. Tolbert, R. B. Kaner, *J. Am. Chem. Soc.* **2005**, *127*, 7264.
- [8] X. Q. Chen, C. L. Fu, M. Krcmar, G. S. Painter, *Phys. Rev. Lett.* **2008**, *100*, 196403.
- [9] T. Ma, H. Li, X. Zheng, S. Wang, X. Wang, H. Zhao, S. Han, J. Liu, R. Zhang, P. Zhu, Y. Long, J. Cheng, Y. Ma, Y. Zhao, C. Jin, X. Yu, *Adv. Mater.* **2017**, *29*, 1604003.
- [10] H. Tang, X. Gao, J. Zhang, B. Gao, W. Zhou, B. Yan, X. Li, Q. Zhang, S. Peng, D. Huang, L. Zhang, X. Yuan, B. Wan, C. Peng, L. Wu, D. Zhang, H. Liu, L. Gu, F. Gao, T. Irifune, R. Ahuja, H. K. Mao, H. Gou, *Chem. Mater.* **2020**, *32*, 459.
- [11] H. Gou, N. Dubrovinskaia, E. Bykova, A. A. Tsirlin, D. Kasinathan, W. Schnelle, A. Richter, M. Merlini, M. Hanfland, A. M. Abakumov, D. Batuk, G. Van Tendeloo, Y. Nakajima, A. N. Kolmogorov, L. Dubrovinsky, *Phys. Rev. Lett.* **2013**, *111*, 157002.
- [12] G. Akopov, W. H. Mak, D. Kouroulis, H. Yin, B. Owens-Baird, M. T. Yeung, M. H. Muni, S. Lee, I. Roh, Z. C. Sobell, P. L. Diaconescu, R. Mohammadi, K. Kovnir, R. B. Kaner, *J. Am. Chem. Soc.* **2019**, *141*, 9047.
- [13] L. Ma, X. Yang, G. Liu, H. Liu, G. Yang, H. Wang, J. Cai, M. Zhou, H. Wang, *Phys. Rev. B* **2021**, *104*, 174112.
- [14] H. Gou, A. A. Tsirlin, E. Bykova, A. M. Abakumov, G. Van Tendeloo, A. Richter, S. V. Ovsyannikov, A. V. Kurnosov, D. M. Trots, Z. Konôpková, H. P. Liermann, L. Dubrovinsky, N. Dubrovinskaia, *Phys. Rev. B* **2014**, *89*, 064108.
- [15] D. Errandonea, R. Boehler, M. Ross, *Phys. Rev. B* **2001**, *65*, 012108.
- [16] S. P. McAlister, E. D. Crozier, J. F. Cochran, *Can. J. Phys.* **1974**, *52*, 1847.
- [17] Y. Ma, M. Eremets, A. R. Oganov, Y. Xie, I. Trojan, S. Medvedev, A. O. Lyakhov, M. Valle, V. Prakapenka, *Nature* **2009**, *458*, 182.
- [18] J. Lv, Y. Wang, L. Zhu, Y. Ma, *Phys. Rev. Lett.* **2011**, *106*, 015503.
- [19] Z. Liu, X. Han, D. Yu, Y. Sun, B. Xu, X. F. Zhou, J. He, H. T. Wang, Y. Tian, *Appl. Phys. Lett.* **2010**, *96*, 031903.
- [20] S. Xin, S. Liu, Z. Zhao, J. Yang, B. Xu, Y. Tian, D. Yu, *Sci. China Phys. Mech.* **2011**, *54*, 1791.
- [21] B. Zhao, X. Wang, L. Yu, Y. Liu, X. Chen, B. Yang, G. Yang, S. Zhang, L. Gu, X. Liu, *Adv. Funct. Mater.* **2021**, *32*, 2110872.
- [22] S. Zhang, X. Du, J. Lin, A. Bergara, X. Chen, X. Liu, X. Zhang, G. Yang, *Phys. Rev. B* **2020**, *101*, 174507.
- [23] Q. Gu, G. Krauss, W. Steurer, *Adv. Mater.* **2008**, *20*, 3620.
- [24] Y. Zhang, L. Wu, B. Wan, Y. Zhao, R. Gao, Z. Li, J. Zhang, H. Gou, H. K. Mao, *Phys. Chem. Chem. Phys.* **2016**, *18*, 2361.
- [25] H. Zhai, F. Munoz, A. N. Alexandrova, *J. Mater. Chem. C* **2019**, *7*, 10700.
- [26] F. Ling, L. Hao, K. Luo, Z. Yuan, Y. Gao, Q. Gao, Y. Li, Z. Zhao, Y. Zhang, D. Yu, *Comput. Mater. Sci.* **2020**, *176*, 109517.
- [27] J. Nagamatsu, N. Nakagawa, T. Muranaka, Y. Zenitani, J. Akimitsu, *Nature* **2001**, *410*, 63.
- [28] Z. Yuan, L. Hao, K. Luo, M. Xiong, C. Shao, F. Ling, D. Yu, *Chem. Phys. Lett.* **2019**, *722*, 80.
- [29] Y. Pan, Y. Jia, *J. Mater. Res.* **2019**, *34*, 3554.
- [30] J. Lei, G. Akopov, M. T. Yeung, J. Yan, R. B. Kaner, S. H. Tolbert, *Adv. Funct. Mater.* **2019**, *29*, 1900293.
- [31] S. Shah, A. N. Kolmogorov, *Phys. Rev. B* **2013**, *88*, 014107.
- [32] A. R. Oganov, C. W. Glass, *J. Chem. Phys.* **2006**, *124*, 244704.
- [33] A. R. Oganov, A. O. Lyakhov, M. Valle, *Acc. Chem. Res.* **2011**, *44*, 227.
- [34] A. O. Lyakhov, A. R. Oganov, H. T. Stokes, Q. Zhu, *Comput. Phys. Commun.* **2013**, *184*, 1172.
- [35] Y. Wang, J. Lv, L. Zhu, Y. Ma, *Phys. Rev. B* **2010**, *82*, 094116.
- [36] Y. Wang, J. Lv, L. Zhu, Y. Ma, *Comput. Phys. Commun.* **2012**, *183*, 2063.
- [37] X. Shao, J. Lv, P. Liu, S. Shen, P. Gao, H. Liu, Y. Wang, Y. Ma, *J. Chem. Phys.* **2022**, *156*, 014105.
- [38] G. Akopov, M. T. Yeung, R. B. Kaner, *Adv. Mater.* **2017**, *29*, 1604506.
- [39] N. P. Salke, M. M. Davari Esfahani, N. Yedukondalu, Y. Zhang, I. A. Kruglov, J. Zhou, E. Greenberg, V. B. Prakapenka, J. Liu, A. R. Oganov, J. F. Lin, *Inorg. Chem.* **2020**, *59*, 5303.
- [40] I. A. Kruglov, A. G. Kvashnin, A. F. Goncharov, A. R. Oganov, S. S. Lobanov, N. Holtgrewe, S. Jiang, V. B. Prakapenka, E. Greenberg, A. V. Yanilkin, *Sci. Adv.* **2018**, *4*, eaat9776.
- [41] D. Li, Y. N. Xu, W. Y. Ching, *Phys. Rev. B* **1992**, *45*, 5895.
- [42] A. R. Oganov, J. Chen, C. Gatti, Y. Ma, Y. Ma, C. W. Glass, Z. Liu, T. Yu, O. O. Kurakevych, V. L. Solozhenko, *Nature* **2009**, *457*, 863.
- [43] A. D. Becke, K. E. Edgecombe, *J. Chem. Phys.* **1990**, *92*, 5397.
- [44] A. Simon, *Angew. Chem., Int. Ed.* **1997**, *36*, 1788.
- [45] Z. Cui, Q. Yang, X. Qu, X. Zhang, Y. Liu, G. Yang, *J. Mater. Chem. C* **2022**, *10*, 672.
- [46] Y. Liang, M. Xu, Z. Qu, S. Lin, J. Hao, Y. Li, *J. Mater. Chem. C* **2021**, *9*, 8258.
- [47] P. B. Allen, R. C. Dynes, *Phys. Rev. B* **1975**, *12*, 905.
- [48] J. Song, G. Fei, X. Liu, S. Duan, B. Yang, X. Chen, D. J. Singh, Y. Liu, L. Yang, J. Guo, P. Zhang, *J. Mater. Chem. A* **2020**, *8*, 20054.
- [49] D. Duan, Y. Liu, F. Tian, D. Li, X. Huang, Z. Zhao, H. Yu, B. Liu, W. Tian, T. Cui, *Sci. Rep.* **2014**, *4*, 6968.
- [50] Y. X. Liu, C. Wang, S. Han, X. Chen, H. R. Sun, X. B. Liu, *Chin. Phys. Lett.* **2021**, *38*.
- [51] Q. Yan, Y. X. Wang, B. Wang, J. Yang, G. Yang, RSC Adv. **2015**, *5*, 25919.
- [52] X. Q. Chen, H. Niu, D. Li, Y. Li, *Intermetallics* **2011**, *19*, 1275.
- [53] F. Gao, J. He, E. Wu, S. Liu, D. Yu, D. Li, S. Zhang, Y. Tian, *Phys. Rev. Lett.* **2003**, *91*, 015502.
- [54] X. Guo, L. Li, Z. Liu, D. Yu, J. He, R. Liu, B. Xu, Y. Tian, H. T. Wang, *J. Appl. Phys.* **2008**, *104*, 023503.
- [55] L. Wu, B. Wan, H. Liu, H. Gou, Y. Yao, Z. Li, J. Zhang, F. Gao, H. K. Mao, *J. Phys. Chem. Lett.* **2016**, *7*, 4898.

- [56] L. Zhu, G. M. Borstad, R. E. Cohen, T. A. Strobel, *Phys. Rev. B* **2019**, 100, 214102.
- [57] L. Hao, X. Li, Y. Zhang, K. Luo, Y. Gao, F. Ling, Y. Wu, Z. Zhao, D. Yu, *Comput. Mater. Sci.* **2019**, 158, 255.
- [58] L. Duan, J. Su, N. Gong, B. Wan, P. Chen, P. Zhou, Z. Wang, Z. Li, L. Wu, *Dalton Trans.* **2019**, 48, 14299.
- [59] C. Fan, Y. Jin, J. Li, X. Dong, *Sci. Rep.* **2014**, 4, 6993.
- [60] H. Xiang, Y. Zhou, *J. Eur. Ceram. Soc.* **2020**, 40, 1352.
- [61] X. L. He, X. Dong, Q. Wu, Z. Zhao, Q. Zhu, A. R. Oganov, Y. Tian, D. Yu, X. F. Zhou, H. T. Wang, *Phys. Rev. B* **2018**, 97, 100102.
- [62] Z. Liu, G. Na, F. Tian, L. Yu, J. Li, L. Zhang, *InfoMat* **2020**, 2, 879.
- [63] G. Kresse, J. Furthmüller, *Comput. Mater. Sci.* **1996**, 6, 15.
- [64] J. P. Perdew, K. Burke, M. Ernzerhof, *Phys. Rev. Lett.* **1996**, 77, 3865.
- [65] G. Kresse, D. Joubert, *Phys. Rev. B* **1999**, 59, 1758.
- [66] H. J. Monkhorst, J. D. Pack, *Phys. Rev. B* **1976**, 13, 5188.
- [67] R. Droroskowski, P. E. Bloechl, *J. Phys. Chem.* **1993**, 97, 8617.
- [68] R. F. W. Bader, *Acc. Chem. Res.* **1985**, 18, 9.
- [69] K. Parlinski, Z. Q. Li, Y. Kawazoe, *Phys. Rev. Lett.* **1997**, 78, 4063.
- [70] A. Togo, F. Oba, I. Tanaka, *Phys. Rev. B* **2008**, 78, 134106.
- [71] P. Giannozzi, S. Baroni, N. Bonini, M. Calandra, R. Car, C. Cavazzoni, D. Ceresoli, G. L. Chiarotti, M. Cococcioni, I. Dabo, A. Dal Corso, S. de Gironcoli, S. Fabris, G. Fratesi, R. Gebauer, U. Gerstmann, C. Gougoussis, A. Kokalj, M. Lazzeri, L. Martin-Samos, N. Marzari, F. Mauri, R. Mazzarello, S. Paolini, A. Pasquarello, L. Paulatto, C. Sbraccia, S. Scandolo, G. Sclauzero, A. P. Seitsonen, et al., *J. Phys.: Condens. Matter* **2009**, 21, 395502.
- [72] G. J. Martyna, M. L. Klein, M. Tuckerman, *J. Chem. Phys.* **1992**, 97, 2635.
- [73] R. Hill, *Pro. Phys. Soc. Sect. A* **1952**, 65, 349.